

Alfvén Wave Collisions, The Fundamental Building Block of Plasma Turbulence II: Numerical Solution

K. D. Nielson,¹ G. G. Howes,^{1, a)} and W. Dorland²

¹*Department of Physics and Astronomy, University of Iowa, Iowa City, Iowa 52242, USA.*

²*Department of Physics, University of Maryland, College Park, Maryland 20742-3511, USA.*

(Dated: 3 July 2018)

This paper presents the numerical verification of an asymptotic analytical solution for the nonlinear interaction between counterpropagating Alfvén waves, the fundamental building block of astrophysical plasma turbulence. The analytical solution, derived in the weak turbulence limit using the equations of incompressible MHD, is compared to a nonlinear gyrokinetic simulation of an Alfvén wave collision. The agreement between these methods signifies that the incompressible solution satisfactorily describes the essential dynamics of the nonlinear energy transfer, even under the weakly collisional plasma conditions relevant to many astrophysical environments.

I. INTRODUCTION

Plasma turbulence impacts the evolution of many space and astrophysical environments of interest, primarily by mediating the transfer of energy from large-scale motions to sufficiently small scales that the turbulence can be dissipated, ultimately leading to heating of the plasma. The turbulent cascade of energy in astrophysical plasmas is driven by nonlinear interactions between counterpropagating Alfvén waves, commonly called Alfvén wave collisions. In our companion paper, Howes and Nielson,¹ hereafter Paper I, we discuss the properties of this fundamental building block of astrophysical plasma turbulence and present an asymptotic analytical solution for the nonlinear evolution of the interaction between two counterpropagating Alfvén waves using the incompressible magnetohydrodynamics (MHD) equations in the weakly nonlinear limit. The primary aim of this paper is to present a numerical verification of this analytical solution.

The incompressible MHD solution for the nonlinear interaction between two counterpropagating Alfvén waves derived in Paper I provides useful insight into the nature of the turbulent cascade of energy in magnetized astrophysical plasmas. Many such astrophysical plasmas, however, do not satisfy the conditions necessary for the validity of the incompressible MHD equations, calling into question the applicability of such an idealized solution. The standard MHD approximation is valid for non-relativistic ($v_i/c \ll 1$), large-scale ($k\rho_i \ll 1$), and low-frequency ($\omega \ll \Omega_i$) motions under strongly collisional plasma conditions ($\omega \ll \nu$). In addition, incompressibility requires a sound speed much larger than the Alfvén speed,¹ or the large plasma beta limit ($\beta \gg 1$). Although the inertial range turbulent dynamics of many space and astrophysical plasmas indeed satisfy the first three conditions, such plasmas are often weakly collisional, $\omega \gg \nu$,

and may have a low or order-unity plasma beta, $\beta \lesssim 1$. We hypothesize here that, *even under weakly collisional conditions with order-unity plasma beta, the nonlinear dynamics between counterpropagating Alfvén waves that underlies the turbulent cascade of energy remains well described by the incompressible MHD solution derived in Paper I.* The secondary aim of this paper is to test this hypothesis by directly comparing the incompressible MHD analytical solution from Paper I to the nonlinear numerical evolution described by gyrokinetics,²⁻⁴ a formalism that rigorously describes the kinetic plasma dynamics in the limit of weak collisionality and order-unity plasma beta. This numerical verification establishes the applicability of the qualitative picture of Alfvén wave collisions described in Paper I to turbulence in realistic space and astrophysical plasma environments of interest.

The gyrokinetic numerical method used to simulate the collision between the Alfvén waves is described in §II. In §III, the numerical solution is presented, with a detailed verification of the predicted time evolution for both the complex Elsasser potentials and the real electromagnetic fields. The results are discussed and conclusions drawn in §IV.

II. NUMERICAL METHOD

To verify the analytical solution derived in Paper I, we perform a nonlinear simulation of the collision between two counterpropagating Alfvén waves using **AstroGK**, the Astrophysical Gyrokinetics Code, developed specifically to study kinetic turbulence in astrophysical plasmas. Although it may seem an unusual choice, the use of a gyrokinetic code to verify an analytical solution derived in the framework of incompressible MHD is a deliberate one.

First, recall from Paper I that the analytical solution presented there is formally valid only in the anisotropic limit, $k_\perp \gg k_\parallel$, a limit that arises naturally in magnetized plasma turbulence, hereafter denoted the *anisotropic limit*. In this anisotropic limit,

^{a)}gregory-howes@uiowa.edu

the low-frequency kinetic dynamics of a weakly collisional plasma is rigorously described by the gyrokinetic system of equations.²⁻⁴ In the limit of perpendicular scales much larger than the ion Larmor radius, $k_{\perp}\rho_i \ll 1$, it has been shown that the Alfvénic dynamics in a weakly collisional plasma is formally governed by the much more simple equations of reduced MHD.⁴ As shown in Paper I, in the anisotropic limit $k_{\perp} \gg k_{\parallel}$, the incompressible MHD description of the Alfvénic dynamics is equivalent to the reduced MHD description. Therefore, we expect that the analytical solution derived in Paper I is valid description of the Alfvénic dynamics described by gyrokinetics in the limit $k_{\perp}\rho_i \ll 1$, hereafter denoted the *MHD limit*.

Second, we choose to verify the analytical solutions with a gyrokinetic code to test our hypothesis that the essential dynamical behavior of the turbulent energy cascade in astrophysical plasma environments is well described using the simplified framework of incompressible MHD. Many of the fundamental concepts that form the foundation of modern theories for plasma turbulence have been derived in the context of incompressible MHD, so it is important to determine if these properties persist under more general plasma conditions in order to establish the applicability of these idealized theoretical concepts to turbulence in real space and astrophysical plasmas. As discussed in the introduction, such astrophysical plasmas are frequently found to be weakly collisional, so a kinetic description of the turbulent dynamics is formally required. In the anisotropic limit that arises naturally in magnetized plasma turbulence, the low-frequency kinetic dynamics of the turbulence is properly captured by a gyrokinetic description.³⁻⁵ Therefore, by using a gyrokinetic code to validate our incompressible MHD solutions for the dynamics of the nonlinear interaction between counterpropagating Alfvén waves, we can determine if the kinetic dynamics of the turbulent energy cascade in weakly collisional space and astrophysical plasmas is adequately described by the much more simple and analytically tractable equations of incompressible MHD. Moreover, in the future, as we extend our investigation to the smaller scales $k_{\perp}\rho_i \gtrsim 1$ where the linear wave physics becomes dispersive, we can explore how the turbulent energy transfer changes character as it transitions from a cascade of nondispersive Alfvén waves to a cascade of dispersive kinetic Alfvén waves.³⁻⁸

A. Numerical Code Description

We use **AstroGK**, the Astrophysical Gyrokinetics Code, to simulate the nonlinear evolution of the collision between counterpropagating Alfvén waves. A detailed description of the algorithms in the code and the results of linear and nonlinear benchmarks are presented in Numata *et al.*⁹, so we give here only a brief overview.

AstroGK evolves the perturbed gyroaveraged distribution function $h_s(x, y, z, \lambda, \varepsilon)$ for each species s , the scalar potential φ , parallel vector potential A_{\parallel} , and the par-

allel magnetic field perturbation δB_{\parallel} according to the gyrokinetic equation and the gyroaveraged Maxwell's equations.^{2,3} The gyroaveraging procedure reduces the three-dimensional velocity space to the components parallel and perpendicular to the equilibrium magnetic field, v_{\parallel} and v_{\perp} ; in the code, a complementary representation of velocity space is chosen using the pitch angle $\lambda = v_{\perp}^2/v^2$ and the energy $\varepsilon = v^2/2$. The domain is a periodic box of size $L_{\perp}^2 \times L_{\parallel}$, elongated along the straight, uniform mean magnetic field, $\mathbf{B}_0 = B_0\hat{\mathbf{z}}$. Note that, in the gyrokinetic formalism, all quantities may be rescaled to any parallel dimension satisfying $L_{\parallel}/L_{\perp} \gg 1$. Uniform Maxwellian equilibria for ions (protons) and electrons are chosen, and the correct mass ratio $m_i/m_e = 1836$ is used. Spatial dimensions (x, y) perpendicular to the mean field are treated pseudospectrally; an upwind finite-difference scheme is used in the parallel direction, z . Collisions are incorporated using a fully conservative, linearized collision operator that includes energy diffusion and pitch-angle scattering.^{10,11}

The perpendicular variation in the simulation is described by a complex Fourier representation in perpendicular wavevector space (k_x, k_y) . The complex Fourier coefficients must satisfy the reality condition, for example, $A_{\parallel}(k_x, k_y) = A_{\parallel}^*(-k_x, -k_y)$. Thus, it is necessary to evolve numerically only the Fourier coefficients in the upper half-plane, $k_y \geq 0$. Note that on the line defined by $k_y = 0$, the Fourier coefficients for $k_x < 0$ are simply the complex conjugates of the Fourier coefficients on the same line with $k_x > 0$. Additionally, the coefficient $(k_x, k_y) = (0, 0)$, corresponding to a DC offset, is absorbed into the background equilibrium conditions and is not evolved. We may therefore restrict our discussion of the nonlinear energy transfer in the perpendicular plane to the energy associated with the complex Fourier coefficients in the upper half-plane, $k_y \geq 0$, with the implicit assumption that coefficients in the lower half-plane are determined by the reality condition.

The model problem solved in Paper I involves the nonlinear interaction between two initially overlapping, perpendicularly polarized, counterpropagating linear Alfvén waves in a periodic domain. To simulate this model problem in the **AstroGK** code requires the capability to initialize the linear kinetic eigenfunction for the Alfvén wave mode, specifying throughout the simulation domain both the electromagnetic potentials ϕ , A_{\parallel} , and δB_{\parallel} and the perturbed gyrokinetic distribution functions h_i and h_e . A specialized module has been written for the **AstroGK** code to accomplish this nontrivial initialization, as described in the Appendix.

III. NUMERICAL SOLUTION

In this section, we present the **AstroGK** numerical solution of the nonlinear interaction between two initially overlapping, perpendicularly polarized, counterpropagating linear Alfvén waves in a periodic domain. We con-

sider a uniform, fully ionized proton and electron plasma with Maxwellian equilibrium distribution functions, a realistic mass ratio $m_i/m_e = 1836$, and a straight, uniform magnetic field $\mathbf{B}_0 = B_0 \hat{\mathbf{z}}$. The plasma parameters are ion plasma beta $\beta_i = 8\pi n_i T_i / B_0^2 = 1$ and ion-to-electron temperature ratio $T_i/T_e = 1$.

To compare with the analytical incompressible MHD solution in Paper I, we must choose a simulation domain suitable for investigating the dynamics in both the anisotropic limit, $k_\perp \gg k_\parallel$, and the MHD limit, $k_\perp \rho_i \ll 1$. The simulation domain $L_\perp^2 \times L_\parallel$ is therefore taken to have a perpendicular width $L_\perp = 80\pi \rho_i$ and is elongated in the direction of the magnetic field such that the gyrokinetic expansion parameter $\epsilon = L_\perp / L_\parallel \ll 1$. Here the ion Larmor radius is defined by $\rho_i = v_{ti} / \Omega_i$, where the ion thermal velocity is $v_{ti}^2 = 2T_i / m_i$, the ion cyclotron frequency is $\Omega_i = q_i B_0 / (m_i c)$, and the Boltzmann constant has been absorbed to give temperature in units of energy. Defining the wavenumbers associated with the domain scale to be $k_\parallel \equiv 2\pi / L_\parallel$ and $k_\perp \equiv 2\pi / L_\perp$, the two initial counterpropagating Alfvén waves will have $k_\perp \rho_i = 0.025$, satisfying the MHD limit, and $k_\parallel / k_\perp = \epsilon \ll 1$, satisfying the anisotropic limit. The characteristic frequency ω_0 of a domain-scale Alfvén wave is given by $\omega_0 = k_\parallel v_A$. The numerical solution to the linear collisionless gyrokinetic dispersion relation gives a real frequency $\omega_r = 1.00131\omega_0$ and damping rate $\gamma = 2.94692 \times 10^{-5}\omega_0$.

The dimensions of the **AstroGK** numerical simulation are $(n_x, n_y, n_z, n_\lambda, n_\epsilon, n_s) = (16, 16, 32, 32, 32, 2)$. The collision frequencies used in the linear relaxation phase (see Appendix) are $\nu_i = 2.3 \times 10^{-4}\omega_0$ and $\nu_e = 6.5 \times 10^{-5}\omega_0$, and in the nonlinear simulation are $\nu_i = 1.1 \times 10^{-5}\omega_0$ and $\nu_e = 3.2 \times 10^{-6}\omega_0$. In the weakly damped MHD regime, the linear relaxation phase requires many periods to eliminate the transient behavior; in this simulation at $k_\perp \rho_i = 0.025$, this phase continues for 150 periods of the initialized Alfvén waves. After relaxation, the linear frequency and damping rate of both of these modes are verified to give values in agreement with the linear collisionless gyrokinetic dispersion relation.

In this simulation, we initialize two overlapping, perpendicularly polarized, counterpropagating linear Alfvén waves, as shown in Figure 1 of Paper I. Given $k_\perp \rho_i = 0.025$ and $k_\parallel / k_\perp \ll 1$, we specify the initial plane wave modes by the shorthand $(k_x/k_\perp, k_y/k_\perp, k_z/k_\parallel) = (1, 0, -1)$ and $(0, 1, 1)$. Note that we maintain the convention established in Paper I that $\omega_0 = k_\parallel v_A > 0$, so that the sign of k_z determines the direction of propagation of the Alfvén wave; therefore, it is clear that the initialized waves are both perpendicularly polarized and counterpropagating.

A critical aspect of the nonlinear simulation is to select the amplitude of the initialized modes to satisfy the ordering assumed in the asymptotic analytical solution in Paper I. For the incompressible MHD equations in the

symmetrized Elsässer form,¹²

$$\frac{\partial \mathbf{z}^\pm}{\partial t} \mp \mathbf{v}_A \cdot \nabla \mathbf{z}^\pm = -\mathbf{z}^\mp \cdot \nabla \mathbf{z}^\pm - \nabla P / \rho_0, \quad (1)$$

this ordering imposes that magnitude of the nonlinear term $\mathbf{z}^\mp \cdot \nabla \mathbf{z}^\pm$ is small compared to the magnitude of the linear term $\mathbf{v}_A \cdot \nabla \mathbf{z}^\pm$. The strength of the nonlinearity affecting the evolution of \mathbf{z}^\pm is conveniently quantified by defining a nonlinearity parameter χ^\pm that is the ratio of the magnitude of the nonlinear term to that of the linear term

$$\chi^\pm \equiv \left| \frac{\mathbf{k}_\perp^\pm \cdot \mathbf{z}^\mp}{k_\parallel^\pm v_A} \right| \quad (2)$$

A nonlinearity parameter $\chi^\pm \sim 1$ signifies the limit of critically balanced, strong turbulence,¹³ where the linear and nonlinear terms have the same magnitude; the limit $\chi^\pm \ll 1$ corresponds to the case of weak turbulence, and is the appropriate case to compare to the analytical solution. Substituting the definition of the Elsässer potentials, $\mathbf{z}^\mp = \hat{\mathbf{z}} \times \nabla_\perp \zeta^\mp$, into (2), we define a characteristic amplitude ζ_{NL}^\mp that corresponds to the case of critically balanced, strong turbulence with $\chi^\pm = 1$, given by

$$\zeta_{NL}^\mp \equiv \frac{k_\parallel^\pm v_A}{\hat{\mathbf{z}} \cdot (\mathbf{k}_\perp^\mp \times \mathbf{k}_\perp^\pm)}. \quad (3)$$

With this definition, the nonlinearity parameter for a counterpropagating Alfvén wave collision is simply given by $\chi^\pm = \zeta^\mp / \zeta_{NL}^\mp$. For the two equal-amplitude, counterpropagating Alfvén waves specified in this simulation, the characteristic amplitudes are the same for both wave directions $\zeta_{NL}^+ = \zeta_{NL}^-$, reducing the expression above to $\zeta_{NL} \equiv k_\parallel v_A / k_\perp^2$. The amplitudes of the initial waves for the simulation are specified to be $\zeta^\mp / \zeta_{NL} = 0.02$, satisfying the ordering assumed in the analytical calculation.

In closing, we state for completeness that the relationship between the Elsässer potentials and the gyrokinetic potentials⁴ is given by

$$\zeta^\pm = \frac{c\phi}{B_0} \mp \frac{A_\parallel}{\sqrt{4\pi n_0 m_i}}. \quad (4)$$

A. Overall Nonlinear Evolution

We begin the presentation of the **AstroGK** numerical solution with an overall picture of the energy transfer due to the nonlinear interaction between two counterpropagating Alfvén waves. In this section, we focus only on the Fourier modes that play a role in the secular transfer of energy to smaller scales, or larger wavenumbers, as described qualitatively in the discussion in §IV A of Paper I. The key modes at each asymptotic order of the analytical solution, presented in Figure 1, are the primary counterpropagating Alfvén waves $(1, 0, -1)$ and $(0, 1, 1)$ (red circles), the secondary inherently nonlinear magnetic

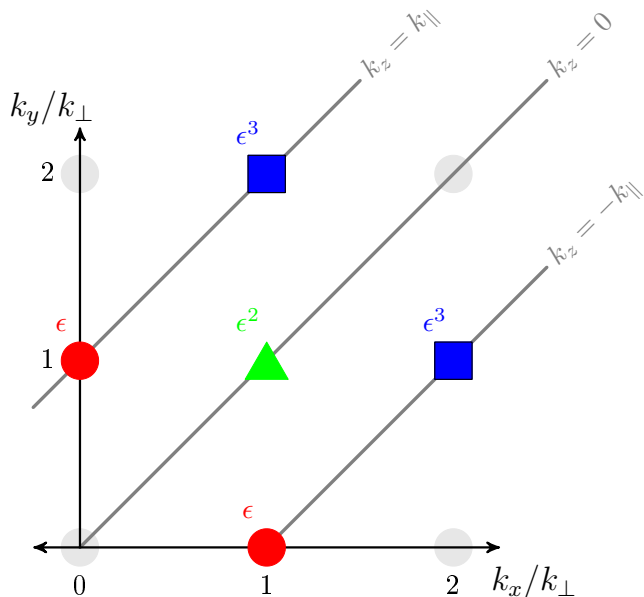


FIG. 1. Schematic diagram of the Fourier modes that play a role in the secular transfer of energy to small scales in an Alfvén wave collision. These key Fourier modes are the primary counterpropagating Alfvén waves (red circles), the secondary inherently nonlinear magnetic field fluctuation (green triangle), and the tertiary counterpropagating Alfvén waves (blue squares). The parallel wavenumber k_z for each of the modes is indicated by the diagonal grey lines, a consequence of the resonance conditions for the wavevector.

field fluctuation $(1, 1, 0)$ (green triangle), and the tertiary counterpropagating Alfvén waves $(2, 1, -1)$ and $(1, 2, 1)$ (blue squares).

The time evolution of the normalized amplitudes of $|\zeta^\pm|/\zeta_{NL}$ for each of these key Fourier modes is shown in Figure 2, demonstrating a number of important qualitative characteristics of the nonlinear evolution. First, note that solutions remain well-ordered throughout the evolution of the simulation, with $|\zeta_1^\pm| \gg |\zeta_2^\pm| \gg |\zeta_3^\pm|$. Therefore, we expect that the asymptotic analytical solution derived Paper I should remain valid over the entire simulation. Second, the due to the weak nonlinearity $\zeta^\pm/\zeta_{NL} = 0.02$, the energy loss from the primary modes (red) is negligible. Third, the second-order mode (green) indeed has a frequency of $2\omega_0$, as expected from the analytical solution. Finally, the secular energy gain by the tertiary modes (blue) leads to an amplitude that increases linearly with time (solid black), $|\zeta_3^\pm| \propto t$, as predicted by the analytical solution.

B. Numerical Validation of Analytical Solution to $\mathcal{O}(\epsilon^3)$

Here we present a thorough validation of the asymptotic analytical solution in Paper I for all of the modes arising up to $\mathcal{O}(\epsilon^3)$. All of these modes are depicted in Figure 2 of Paper I, which shows both the key Fourier modes shown here in Figure 1 and the Fourier modes

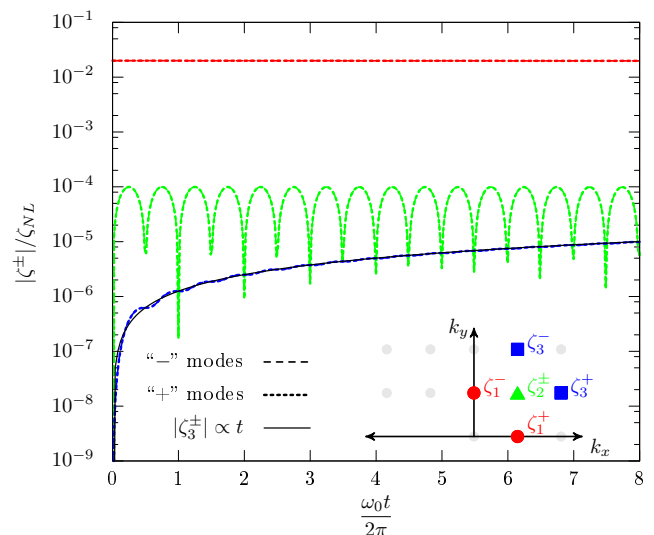


FIG. 2. Evolution of the normalized amplitude $|\zeta^\pm|/\zeta_{NL}$ of the key Fourier modes vs. time $\omega_0 t/2\pi$ over eight periods of the primary Alfvén waves. The color map is the same as Figure 1, and a linear increase with time is indicated by the solid black line.

at $k_x < 0$ that do not play a role in the secular energy transfer. In Figure 3, we plot the real (black) and imaginary (red) components of the complex Elsasser potentials ζ_n^\pm at orders $n = 1, 2, 3$ from the asymptotic analytical solution (dotted) and gyrokinetic numerical simulation (dashed). The left panel presents the modes with $k_x > 0$ that play a role in the secular energy transfer to small scales, and the right panel presents the modes with $k_x < 0$ that do not play a role in this energy transfer. All modes with $k_x > 0$ (panels a–f) show excellent agreement between the asymptotic analytical solution and the gyrokinetic numerical simulation. The modes with $k_x < 0$ (panels g–l) show that a phase difference arises over time between the analytical and numerical solutions. The cause of this minor discrepancy is not clear, but may be due to higher-order effects not included in the incompressible MHD solution arising from finite Larmor radius corrections. Note, however, the amplitude of the third order solutions in Figure 3 (lower two rows across both panels) demonstrates that the modes in panels (c) and (f) dominate the energy in the tertiary solutions, and both of these modes show excellent agreement with the analytical predictions. Therefore, the minor phase differences that arise for the $k_x < 0$ modes do not suggest an energetically significant deviation from the analytical solution.

C. Physical Representation of the Solution in **B** and **E**

Although the comparison of the nonlinear evolution of the analytical and numerical complex Elsasser potentials in §III B provides a thorough validation of the analyt-

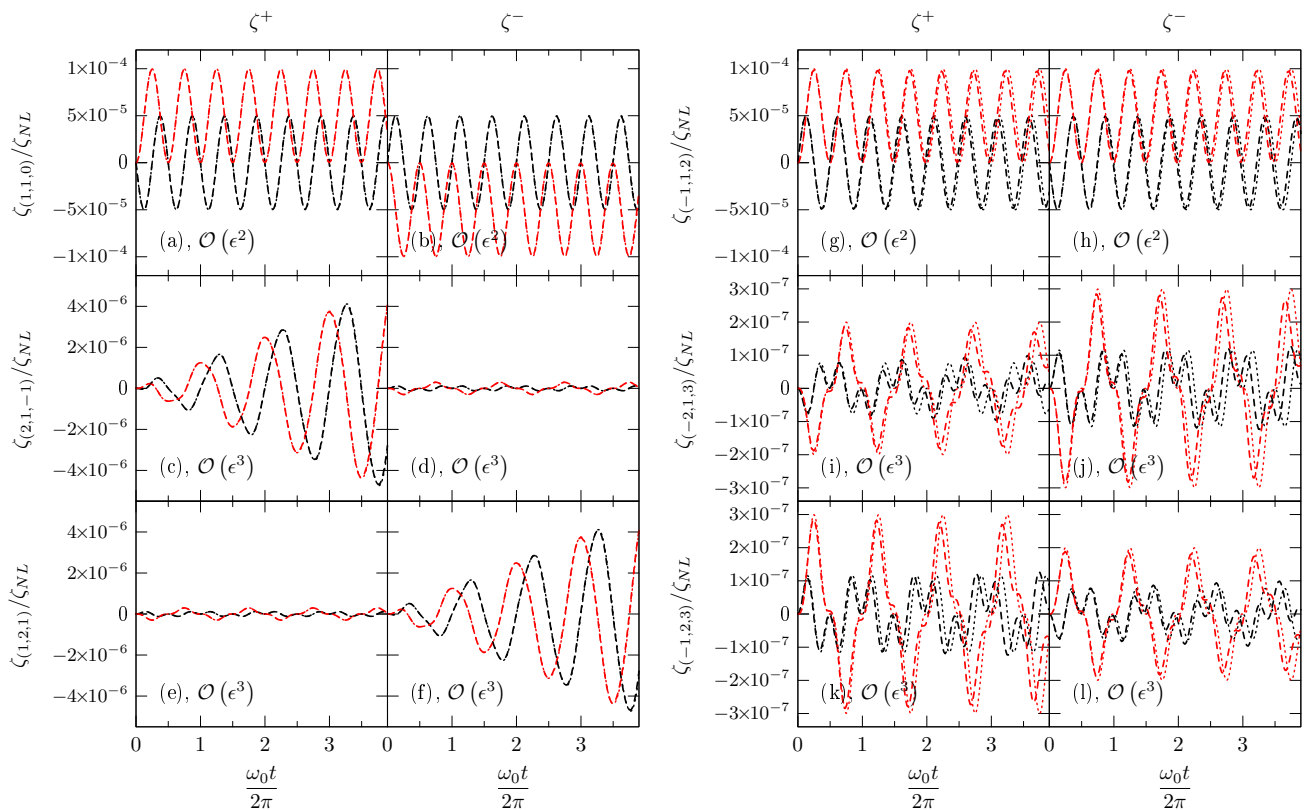


FIG. 3. A comparison of the real (black) and imaginary (red) components of the complex Elsasser potentials ζ_n^\pm at orders $n = 1, 2, 3$ from the asymptotic analytical solution (dotted) and gyrokinetic numerical simulation (dashed).

ical solution, it does not immediately provide a simple intuitive picture of the dynamical evolution of the turbulent electromagnetic fields. Since it is the real electromagnetic fields that are measured directly in a turbulent plasma, examining this evolution is of vital importance. Therefore, we present here a complementary comparison between the analytical and numerical solutions of the evolution of the magnetic and electric field fluctuations. In Paper I, the secondary $\mathcal{O}(\epsilon^2)$ solutions for $\mathbf{B}_{\perp 2}$ and $\mathbf{E}_{\perp 2}$ are given by (36) and (37), and the tertiary $\mathcal{O}(\epsilon^3)$ solutions for $\mathbf{B}_{\perp 3}$ and $\mathbf{E}_{\perp 3}$ are given by (40) and (41).

The second order $\mathcal{O}(\epsilon^2)$ asymptotic solution consists of two Fourier modes $(1, 1, 0)$ and $(-1, 1, 2)$ according to (36) and (37) of Paper I. The normalized amplitude of the magnetic field $|\mathbf{B}_{\perp 2}|/B_0$ is plotted in the top panel of Figure 4 for the $(1, 1, 0)$ mode (black) and $(-1, 1, 2)$ mode (red) from both the analytical calculation (dotted) and the numerical solution (dashed). Similarly, the normalized amplitude of the electric field $|\mathbf{E}_{\perp 2}|/(v_A B_0/c)$ is plotted in the bottom panel of Figure 4 for the $(1, 1, 0)$ mode (black) and $(-1, 1, 2)$ mode (red) from both the analytical calculation (dotted) and the numerical solution (dashed). The $\mathcal{O}(\epsilon^2)$ nonlinear response in Figure 4 is purely oscillatory, with no secular energy transfer of energy at this order. The $(1, 1, 0)$ mode solutions agree excellently, with only a magnetic field response and no corresponding electric field response—this is the inher-

ently nonlinear $k_z = 0$ magnetic fluctuation at $\mathcal{O}(\epsilon^2)$ that plays the crucial role in the secular energy transfer to the tertiary $\mathcal{O}(\epsilon^3)$ Alfvén waves, as emphasized in Paper I. The $(-1, 1, 2)$ modes also agree very closely initially, but eventually a small phase shift arises between the numerical and analytical solution, similar to that seen in Figure 3.

Using trigonometric addition formulas, the form of the time dependence of the amplitude of the $\mathcal{O}(\epsilon^2)$ modes can be written as

$$|\mathbf{B}_{\perp 2, (1, 1, 0)}| \propto \sqrt{1 - \cos(2\omega_0 t)}, \quad (5)$$

$$|\mathbf{B}_{\perp 2, (-1, 1, 2)}| \propto |\sin(2\omega_0 t)|, \quad (6)$$

$$|\mathbf{E}_{\perp 2, (1, 1, 0)}| = 0, \quad (7)$$

$$|\mathbf{E}_{\perp 2, (-1, 1, 2)}| \propto 1 - \cos(2\omega_0 t). \quad (8)$$

The third order $\mathcal{O}(\epsilon^3)$ of the asymptotic solution in Paper I is given by (40) and (41) and consists of two Fourier modes $(2, 1, -1)$ and $(1, 2, 1)$ whose amplitudes increase secularly, and four Fourier modes that display oscillatory behavior, $(-2, 1, 3)$, $(-1, 2, 3)$, $(0, 1, 1)$, and $(1, 0, -1)$. Below we present a comparison between the analytical and numerical solutions for the first four Fourier modes;

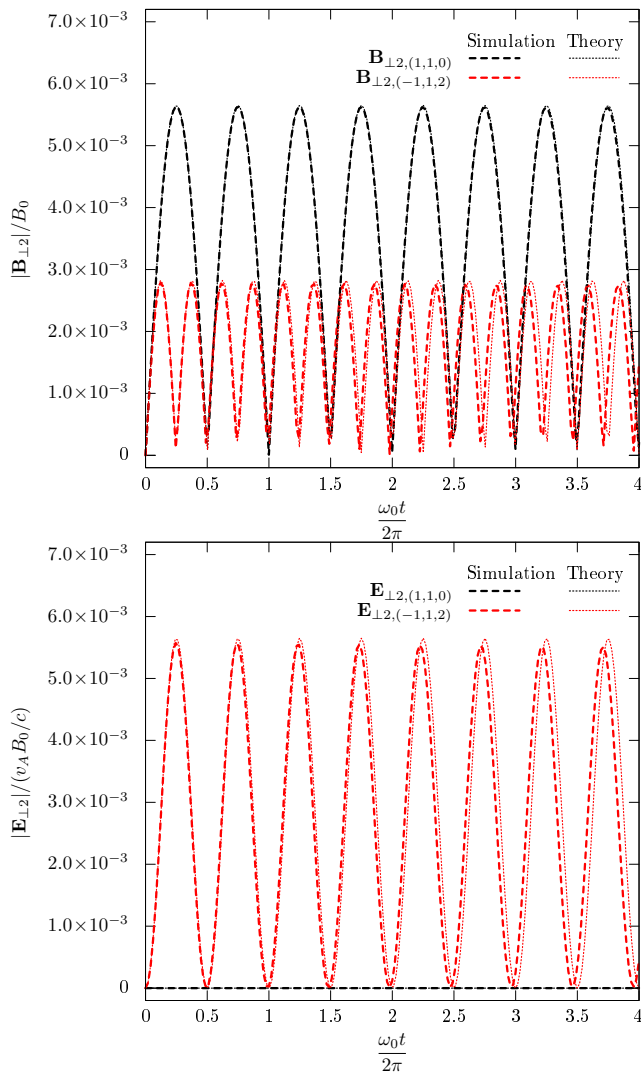


FIG. 4. Comparison of the analytical (dotted) and numerical (dashed) solutions for the time evolution of the amplitude of the magnetic and electric fields at $\mathcal{O}(\epsilon^2)$. The top panel shows the normalized amplitude of the magnetic field $|\mathbf{B}_{\perp 2}|/B_0$ for the $(1, 1, 0)$ mode (black) and $(-1, 1, 2)$ mode (red). The bottom panel shows the normalized amplitude of the electric field $|\mathbf{E}_{\perp 2}|/(v_A B_0/c)$ for the $(1, 1, 0)$ mode (black) and $(-1, 1, 2)$ mode (red).

the latter two modes, $(0, 1, 1)$ and $(1, 0, -1)$, merely represent $\mathcal{O}(\epsilon^3)$ corrections to the primary wave amplitudes and will not be considered further.

The energetically dominant $\mathcal{O}(\epsilon^3)$ Fourier modes are the two modes, $(2, 1, -1)$ and $(1, 2, 1)$, that receive a secular transfer of energy through the nonlinear interaction. As discussed in Paper I, these two modes are Alfvén waves with the same value of k_z as the two primary Alfvén waves, indicating no parallel cascade of energy, but a higher value of the perpendicular component of the wavenumber. The transfer of energy to these tertiary $\mathcal{O}(\epsilon^3)$ Alfvén waves represents the nonlinear cascade of energy to smaller scales that is the most important effect

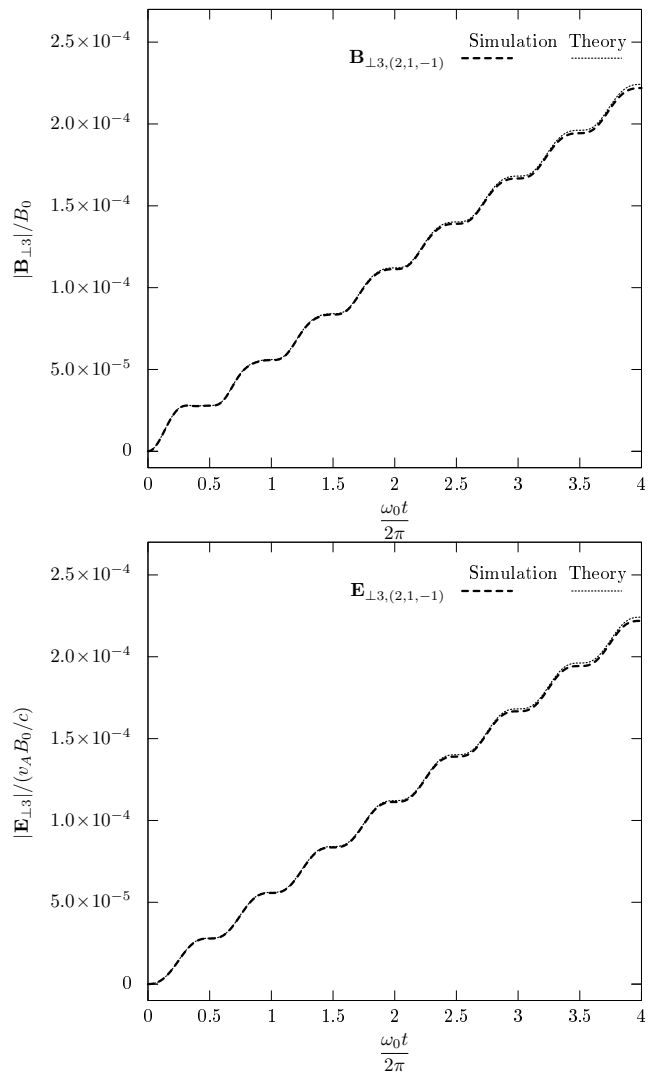


FIG. 5. Comparison of the analytical (dotted) and numerical (dashed) solutions for the time evolution of the amplitude of the magnetic (top) and electric (bottom) fields of the $(2, 1, -1)$ Fourier mode at $\mathcal{O}(\epsilon^3)$.

of turbulence in astrophysical plasmas. In Figure 5, we plot the analytical (dotted) and numerical (dashed) solutions of the normalized amplitude of the magnetic field $|\mathbf{B}_{\perp 2}|/B_0$ (top panel) and electric field $|\mathbf{E}_{\perp 2}|/(v_A B_0/c)$ (bottom panel) for the $(2, 1, -1)$ mode. The agreement between the analytical and numerical solution is seen to be excellent for both fields. Note that, by the inspection of (40) and (41) from Paper I, it is clear that the evolution of the $(1, 2, 1)$ mode has the same form as that for the $(2, 1, -1)$ mode, only with the electric and magnetic fields swapped; therefore, we do not provide a separate plot for the $(1, 2, 1)$ mode, but note that the agreement is the same as that shown in Figure 5.

An important dynamical feature of the nonlinear energy transfer to small scales is evident in Figure 5. As discussed in Paper I, the purely magnetic $(1, 1, 0)$ mode of the $\mathcal{O}(\epsilon^2)$ solution plays a crucial role in the secular

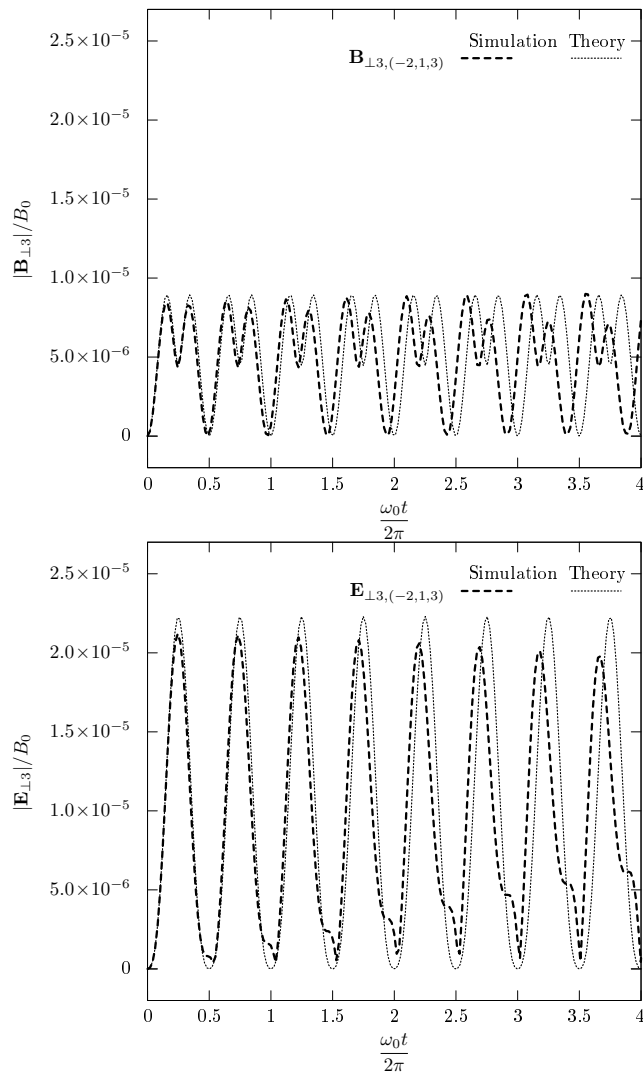


FIG. 6. Comparison of the analytical (dotted) and numerical (dashed) solutions for the time evolution of the amplitude of the magnetic (top) and electric (bottom) fields of the $(-2, 1, 3)$ Fourier mode at $\mathcal{O}(\epsilon^3)$.

energy transfer from the primary $(0, 1, 1)$ and $(1, 0, -1)$ Alfvén waves to the tertiary $(2, 1, -1)$ and $(1, 2, 1)$ Alfvén waves. It is evident, upon examination of the time evolution of the $(1, 1, 0)$ mode in Figure 4 and of the $(2, 1, -1)$ mode in Figure 5, that the amplitude of the $(2, 1, -1)$ mode increases only at times when the $(1, 1, 0)$ mode has non-zero amplitude. Conversely, at times $\omega_0 t / 2\pi = n/2$ for $n = 0, 1, 2, \dots$, when the amplitude of the secondary $(1, 1, 0)$ mode is zero, the amplitude of the $(2, 1, -1)$ mode does not increase. This feature of the solution highlights the essential role played by the inherently nonlinear, purely magnetic, secondary $(1, 1, 0)$ mode in the secular transfer of energy to small scales.

To complete our comparison of the analytical and numerical solutions for the magnetic and electric field evolution, we turn our attention to the nonlinear response of the $(-2, 1, 3)$ and $(-1, 2, 3)$ Fourier modes in the $\mathcal{O}(\epsilon^3)$

solution. In Figure 6, we plot the analytical (dotted) and numerical (dashed) solutions of the normalized amplitude of the magnetic field $|\mathbf{B}_{\perp 2}|/B_0$ (top panel) and electric field $|\mathbf{E}_{\perp 2}|/(v_A B_0/c)$ (bottom panel) for the $(-2, 1, 3)$ mode. Although agreement with the analytical solution at early times is excellent, a phase shift and alteration of the form of the solution arises after several primary wave periods. Note that the solutions for the magnetic and electric field evolution of the $(-1, 2, 3)$ Fourier mode is the same as the $(-2, 1, 3)$ mode presented in Figure 6.

IV. DISCUSSION AND CONCLUSION

In Paper I, we have derived an asymptotic analytical solution for the nonlinear interaction between two initially overlapping, perpendicularly polarized, counter-propagating linear Alfvén waves in the weakly nonlinear limit. The incompressible MHD solution to this idealized problem provides valuable intuition into the fundamental nature of the nonlinear transfer of energy to small scales in magnetized plasma turbulence. The incompressible MHD solution in Paper I is formally rigorous in the anisotropic limit, $k_{\perp} \gg k_{\parallel}$; in this anisotropic limit, the incompressible MHD solution is equivalent to a reduced MHD solution for the Alfvénic dynamics. The primary aim of this companion paper is to present a thorough numerical verification of the analytical solution using the gyrokinetic code `AstroGK` in the MHD limit, $k_{\perp} \rho_i \ll 1$.

The numerical validation shows excellent agreement between the analytical solution and the nonlinear gyrokinetic simulation results for the Fourier modes that play a role in the secular transfer of energy from the primary Alfvén waves to the tertiary Alfvén waves, as depicted in Figure 1. For the Fourier modes with $k_x < 0$, modes that do not play a role in this secular energy transfer, the agreement is very good at early times, but a small phase shift arises after several periods of the primary waves. This minor discrepancy may arise through dispersive effects due to finite Larmor radius corrections that are included in the gyrokinetic simulation but not in the incompressible MHD solution. We note, however, that the modes suffering this small phase shift are energetically subdominant to the modes that receive the secular transfer of energy from the primary Alfvén waves. In summary, the results presented here verify the analytical solution derived in Paper I, accomplishing the primary aim of this paper.

The numerical solution presented here illustrates a couple of salient features of the nonlinear energy transfer. First, as evident in Figure 2, the lowest order of the solution displaying a secular increase of energy is $\mathcal{O}(\epsilon^3)$. As discussed at length in Paper I, this is a consequence of the fact that the energy transfer is due to a resonant, four-wave interaction. Second, also seen in Figure 2, the secular increase of amplitude of these tertiary modes is linear in time, corresponding to an increase in energy $\propto t^2$. Apparently inconsistent with the expectation from scaling

theories of turbulence, this characteristic scaling follows from the coherent nature of the interaction between the primary counterpropagating Alfvén waves. For a more realistic picture of plasma turbulence involving the cumulative effect of successive nonlinear interactions between many uncorrelated Alfvén wave packets, accounting for a random walk in energy changes the scaling of the increase in energy to $\propto t$, as expected from turbulence theories.

The secondary aim of this paper is to test the hypothesis that the physical mechanism for nonlinear energy transfer in plasma turbulence under astrophysically relevant conditions remains well described by the incompressible MHD solution derived in Paper I. In particular, turbulent astrophysical plasmas are often found both to be weakly collisional and to have a typical plasma beta $\beta \lesssim 1$, two limits in which the equations of incompressible MHD are formally invalid. To test this hypothesis, we compare the analytical incompressible MHD solution to numerical gyrokinetic solution in the MHD limit, $k_{\perp}\rho_i \ll 1$, using the Astrophysical Gyrokinetics code, **AstroGK**. Since the gyrokinetic equations rigorously describe the low-frequency kinetic dynamics of the turbulence in the anisotropic limit, the demonstrated agreement between the two methods signifies that, indeed, the incompressible MHD solution satisfactorily describes, in a simple analytical form, the essential dynamics of the nonlinear energy transfer in a turbulent, weakly collisional plasma.

This result was anticipated by the theoretical finding⁴ that the equations of reduced MHD rigorously describe the kinetic dynamics of the turbulent Alfvénic fluctuations in the limit $k_{\perp}\rho_i \ll 1$. Such a surprising simplification of the kinetic dynamics to a fluid limit can be understood physically as resulting from the incompressible nature of Alfvén waves in the limit $k_{\perp}\rho_i \ll 1$. Since Alfvén waves have no associated motions parallel to the magnetic field, the plasma collisionality has influence on neither the linear nor the nonlinear dynamics of Alfvénic fluctuations.

In conclusion, we have numerically verified the asymptotic analytical solution in Paper I¹ for the nonlinear interaction between counterpropagating Alfvén waves in the weakly nonlinear limit. In addition, by comparing the analytical incompressible MHD solution to numerical gyrokinetic solution, we have confirmed the hypothesis that the physical mechanism underlying the nonlinear energy transfer in plasma turbulence under astrophysically relevant conditions remains well described by the simple fluid description of incompressible MHD.

These findings motivate a simplified picture for describing the very complex phenomenon of turbulence in a kinetic plasma. The development of a thorough understanding of kinetic turbulence, a key goal of the space physics and astrophysics communities, requires the elucidation of (1) the fundamental physical mechanisms underlying the nonlinear energy transfer from large to small scales, (2) the dissipation of the turbulent fluctuations at small scales, and (3) the ultimate conversion of the

turbulent energy into plasma heat. Our findings suggest that illuminating the nonlinear wave-wave interactions responsible for the turbulent cascade of energy from large to small scales does not necessarily require a kinetic treatment, but that the dynamics can be satisfactorily described using a reduced fluid description. In the MHD limit, $k_{\perp}\rho_i \ll 1$, we have proven here that the incompressible MHD solution is sufficient; for the limit of a turbulent kinetic Alfvén wave cascade, $k_{\perp}\rho_i \gg 1$, an appropriate fluid description, such as electron reduced MHD,⁴ may be sufficient to describe the nonlinear wave-wave interactions underlying the turbulent energy transfer in this regime. On the other hand, the physical mechanisms in kinetic turbulence responsible for the dissipation and thermalization of the turbulent energy almost certainly do require a kinetic description. The closures for dissipation typically used in fluid descriptions, such as viscosity and resistivity, are not valid in the weakly collisional limit relevant to turbulent dissipation in space and astrophysical plasmas. Instead, inherently kinetic mechanisms, such as collisionless wave-particle interactions and infrequent particle collisions, are almost certainly responsible for the damping of the turbulent fluctuations and the ultimate conversion of their energy into plasma heat.^{3-5,7,8,14}

Based on these arguments, we propose the following simplified framework for understanding kinetic plasma turbulence: (a) nonlinear wave-wave interactions are responsible for the turbulent cascade of energy from large to small scales, and can be adequately described using an appropriate fluid description; (b) kinetic mechanisms, such as collisionless wave-particle interactions, are responsible for the damping of the turbulent electromagnetic fluctuations, requiring a kinetic description; and, (c) thermalization of the free energy in the particle distribution functions, a consequence of the wave-particle interactions above, requires particle collisions to increase entropy and realize irreversible thermodynamic heating,³ a process mediated by an inherently kinetic entropy cascade.^{4,15}

The findings presented here and in Paper I present a simple picture of the nonlinear energy transfer in Alfvén wave collisions, establish the validity of the derived incompressible MHD solution, and demonstrate its relevance to turbulence in astrophysical plasmas in the weakly nonlinear limit. These analytical and numerical solutions have played an invaluable role in the design of an experiment to measure the nonlinear interaction between counterpropagating Alfvén waves in the laboratory.¹⁶ Future extensions of this work will determine whether the essential characteristics of the nonlinear energy transfer persist into the important regime of strong turbulence. In addition, we aim to explore how the nature of the nonlinear energy transfer changes as the turbulent cascade to small scales enters the dispersive regime of kinetic Alfvén waves.

ACKNOWLEDGMENTS

This work was supported by NSF PHY-10033446, NSF CAREER AGS-1054061, and NASA NNX10AC91G. Computing resources were supplied through DOE INCITE Award PSS002, NSF TeraGrid Award PHY090084, and DOE INCITE Award FUS030.

Appendix A: Eigenfunction Initialization and Transient Elimination

In this appendix, we describe the procedure for initialization of linear gyrokinetic eigenfunctions and for the elimination of transient behavior in the initialized modes.

First, the plane wave mode to be initialized is chosen by specifying its wavevector $\mathbf{k} = k_x \hat{\mathbf{x}} + k_y \hat{\mathbf{y}} + k_z \hat{\mathbf{z}}$ and providing an initial guess for the complex frequency $\omega = \omega_r - i\gamma$ of the mode. This guess for the frequency is necessary to ensure that the correct linear wave mode is initialized—in the MHD limit of gyrokinetics, both Alfvén waves and kinetic slow waves¹⁷ are possible, as well as a non-propagating entropy mode. For the problem at hand, we specify that both initialized modes are Alfvén waves. Second, the code employs a numerical solver for the linear, collisionless, gyrokinetic dispersion relation³ to solve for the complex eigenfrequency ω and the complex Fourier coefficients for the eigenfunctions of the electromagnetic potentials $\hat{\phi}$, \hat{A}_{\parallel} and $\delta\hat{B}_{\parallel}$, where the hat symbol denotes the Fourier coefficient. Third, these coefficients are used to initialize at $t = 0$ the electromagnetic potentials on the numerical grid according to $\hat{A}_{\parallel}(k_x, k_y, z, t) = \hat{A}_{\parallel}(k_x, k_y) \exp(ik_z z - i\omega t + i\delta)$, where δ allows for an arbitrary adjustment to the phase of each initialized wave. Fourth, these initial values of the electromagnetic potentials and the complex eigenfrequency are used to compute the complex Fourier coefficients in the perpendicular plane of the perturbed gyrokinetic distribution functions \hat{h}_i and \hat{h}_e , according to the eq (C6) in Howes *et al.*³ Note that these five-dimensional gyrokinetic distribution functions are functions of not only the three spatial coordinates (k_x, k_y, z) but also the two coordinates of gyroaveraged velocity space, v_{\perp} and v_{\parallel} . The generic functional form is therefore $\hat{h}_s(k_x, k_y, z, \lambda, \varepsilon) = \hat{h}_s \left[\omega, \hat{\phi}(k_x, k_y, z), \hat{A}_{\parallel}(k_x, k_y, z), \delta\hat{B}_{\parallel}(k_x, k_y, z), v_{\perp}, v_{\parallel} \right]$. This completes the initialization of a single plane wave mode; additional modes to be initialized may be added by linear superposition.

Thorough testing of this exact linear eigenfunction initialization module has exposed a transient behavior of the initialized mode that does not follow the expectations from the linear theory. There exist two potential causes for this transient behavior. First, the eigenfunction is computed by the numerical solution of an analytical form for the linear dispersion relation which assumes a continuous representation of the distribution functions in velocity space, yet the numerical representation of velocity

space in `AstroGK` is discrete. Therefore, transient behavior that does not follow the linear analytical theory may arise from slight differences between the eigenfunctions in discrete and continuous velocity-space representations. Second, the linear dispersion relation that is solved is collisionless, yet a non-zero collisionality is always employed in `AstroGK` to maintain resolved structures in velocity space,^{7,18} and finite collisionality may lead to deviations of the weakly collisional eigenfunctions in the numerical code from the collisionless eigenfunctions in the analytical theory. Whatever the cause of this transient behavior, a simple procedure has been developed that quickly and effectively allows the initialized modes to relax to behavior consistent with the linear theory, as detailed below.

To eliminate the transient behavior, it suffices to perform a linear relaxation of the initialized mode by running `AstroGK` in linear mode (with the nonlinear terms turned off) with an enhanced collisionality for a number of wave periods sufficient to eliminate this transient behavior. This enhanced collisionality effectively eliminates the deviations of the initialized eigenfunction from the eigenfunction that is appropriate for the discrete, weakly collisional representation in the `AstroGK`. Consider a linear collisionless gyrokinetic wave mode that has real frequency ω_r and damping rate $\gamma = \gamma_i + \gamma_e$, where γ_s is the collisionless damping rate due to the Landau resonance with species s . `AstroGK` simulations are typically run with collisionalities set to values of $\nu_s \leq 0.5\gamma_s$. A value of collisionality of $\nu_s = 0.5\gamma_s$ is sufficiently high to ensure that the structure in velocity space that is generated by wave-particle interactions remains resolved^{7,18} but sufficiently low that the measured damping rate of the mode agrees with the collisionless value. For the linear relaxation phase, we apply an enhanced collisionality with a value $\nu_s = 10\gamma_s$. The linear relaxation continues until a simple exponential damping rate γ for the mode is achieved. After completion of the linear relaxation, tests show that the resulting mode has a frequency and damping rate in close agreement with the prediction of the linear, collisionless dispersion relation. These modes are then used to begin the nonlinear simulation of the counterpropagating Alfvén wave collision. Note that, for Alfvén waves in the MHD limit, for which collisionless damping is weak, $\gamma \ll \omega_r$, even the enhanced collisionality of the linear relaxation phase corresponds to weakly collisional dynamics since $\nu \ll \omega_r$.

¹G. G. Howes and K. D. Nielson, “Alfvén Wave Collisions, The Fundamental Building Block of Plasma Turbulence I: Asymptotic Solution,” *Phys. Plasmas* (2013), submitted.

²E. A. Frieman and L. Chen, “Nonlinear gyrokinetic equations for low-frequency electromagnetic waves in general plasma equilibria,” *Phys. Fluids* **25**, 502–508 (Mar. 1982).

³G. G. Howes, S. C. Cowley, W. Dorland, G. W. Hammett, E. Quataert, and A. A. Schekochihin, “Astrophysical Gyrokinetics: Basic Equations and Linear Theory,” *Astrophys. J.* **651**, 590–614 (Nov. 2006), astro-ph/0511812.

⁴A. A. Schekochihin, S. C. Cowley, W. Dorland, G. W. Hammett, G. G. Howes, E. Quataert, and T. Tatsuno, “Astrophysical Gyrokinetics: Kinetic and Fluid Turbulent Cascades in Magnetized

- Weakly Collisional Plasmas,” *Astrophys. J. Supp.* **182**, 310–377 (May 2009).
- ⁵G. G. Howes, S. C. Cowley, W. Dorland, G. W. Hammett, E. Quataert, and A. A. Schekochihin, “A model of turbulence in magnetized plasmas: Implications for the dissipation range in the solar wind,” *J. Geophys. Res.* **113**, A05103 (May 2008), arXiv:0707.3147.
- ⁶G. G. Howes, W. Dorland, S. C. Cowley, G. W. Hammett, E. Quataert, A. A. Schekochihin, and T. Tatsuno, “Kinetic Simulations of Magnetized Turbulence in Astrophysical Plasmas,” *Phys. Rev. Lett.* **100**, 065004 (Feb. 2008).
- ⁷G. G. Howes, J. M. TenBarge, W. Dorland, E. Quataert, A. A. Schekochihin, R. Numata, and T. Tatsuno, “Gyrokinetic simulations of solar wind turbulence from ion to electron scales,” *Phys. Rev. Lett.* **107**, 035004 (2011).
- ⁸G. G. Howes, J. M. TenBarge, and W. Dorland, “A weakened cascade model for turbulence in astrophysical plasmas,” *Phys. Plasmas* **18**, 102305 (2011), arXiv:1109.4158 [astro-ph.SR].
- ⁹R. Numata, G. G. Howes, T. Tatsuno, M. Barnes, and W. Dorland, “AstroGK: Astrophysical gyrokinetics code,” *J. Comp. Phys.* **229**, 9347 (2010), arXiv:1004.0279 [physics.plasm-ph].
- ¹⁰I. G. Abel, M. Barnes, S. C. Cowley, W. Dorland, and A. A. Schekochihin, “Linearized model Fokker-Planck collision operators for gyrokinetic simulations. I. Theory,” *Phys. Plasmas* **15**, 122509+ (Dec. 2008), arXiv:0808.1300.
- ¹¹M. Barnes, I. G. Abel, W. Dorland, D. R. Ernst, G. W. Hammett, P. Ricci, B. N. Rogers, A. A. Schekochihin, and T. Tatsuno, “Linearized model Fokker-Planck collision operators for gyrokinetic simulations. II. Numerical implementation and tests,” *Phys. Plasmas* **16**, 072107+ (Jul. 2009).
- ¹²W. M. Elsasser, “The Hydromagnetic Equations,” *Physical Review* **79**, 183 (Jul. 1950).
- ¹³P. Goldreich and S. Sridhar, “Toward a Theory of Interstellar Turbulence II. Strong Alfvénic Turbulence,” *Astrophys. J.* **438**, 763–775 (1995).
- ¹⁴J. M. TenBarge and G. G. Howes, “Current Sheets and Collisionless Dissipation in Kinetic Plasma Turbulence,” *Astrophys. J. Lett.* (2012), submitted.
- ¹⁵T. Tatsuno, A. A. Schekochihin, W. Dorland, G. Plunk, M. A. Barnes, S. C. Cowley, and G. G. Howes, “Nonlinear phase mixing and phase-space cascade of entropy in gyrokinetic plasma turbulence,” *Phys. Rev. Lett.* **103**, 015003 (2009).
- ¹⁶G. G. Howes, D. J. Drake, K. D. Nielson, T. A. Carter, C. A. Kletzing, and F. Skiff, “Toward Astrophysical Turbulence in the Laboratory,” *Phys. Rev. Lett.* **109**, 255001 (Dec. 2012), arXiv:1210.4568 [physics.plasm-ph].
- ¹⁷K. G. Klein, G. G. Howes, J. M. TenBarge, S. D. Bale, C. H. K. Chen, and C. S. Salem, “Using Synthetic Spacecraft Data to Interpret Compressible Fluctuations in Solar Wind Turbulence,” *Astrophys. J.* **755**, 159 (2012), arXiv:1206.6564 [physics.space-ph].
- ¹⁸M. Barnes, W. Dorland, and T. Tatsuno, “Resolving velocity space dynamics in continuum gyrokinetics,” *Phys. Plasmas* **17**, 032106 (Mar. 2010), arXiv:0907.4413 [physics.plasm-ph].